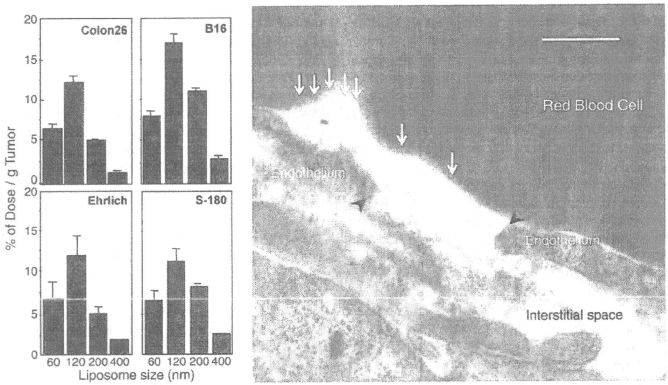

Fig. 1. *Left*: Effect of liposome size on the extravasation of PEG-liposomes into tumor tissue. Liposomes were injected into tumor-bearing mice via the tail vein and biodistribution was investigated at 6 h after injection. Tumor-bearing mice were prepared by inoculating tumor cells ($\sim 1 \times 10^7$) s.c. and were tested when the tumor mass volume reached about 1000–1500 mm^3. *Right*: Electron micrographs showing extravasation and localization of PEG-liposomes (126 ± 35 nm mean diameter) in Colon 26 solid tumor tissue. Liposomes were injected into mice via the tail vein, and the ultrathin sections of tumor tissue were prepared at 24 hr after administration. Between arrowheads : the gap between adjacent endothelial cells, Arrows : liposomes across the gap. Bar = 500 nm.

Caelyx (PEG-liposomal formulation), Myocet (conventional liposomal formulation) and free doxorubicin. Data from representative studies of Hamilton et al. [35], Gabizon et al. [36] and Mross et al. [37], were normalized using an average body surface area of 1.7 m^2 and an average body weight of 70 kg. As shown in Table 2, there are significant differences between the different formulation principles. Doxil/Caelyx shows minimal interaction with non-diseased tissues, leading to both a low systemic plasma clearance as well as a low volume of distribution of 0.03–0.05 L/kg. Consequently, Doxil/Caelyx shows a significantly lower risk of cardiotoxicity [38]. A reduced distribution of liposomal anthracyclines to heart muscle is observed using PEG-liposomes. This site avoidance of a drug-sensitive tissue is paralleled by enhanced drug deposition in tumor tissue (passive tumor targeting) leading to a pharmacodynamic advantage compared to the free drug [39]. Thus, the improved therapeutic index arises from both enhanced efficacy and reduced toxicity.

4. Active targeting of the liposomal carrier to solid tumor

Passive targeting of liposomal drugs to the solid tumor tissue can be achieved by the so called EPR effect. Their specificity can be markedly enhanced when tumor targeting ligands are used. Among the various approaches to active targeting, immunoliposomes using an antibody as a targeting ligand and a lipid vesicle as a carrier for both hydrophobic and hydrophilic drugs have attracted much attention [40,41]. Studies have revealed *in vivo* that coating liposomes with antibody leads to enhanced uptake of the immunoliposomes by the RES [42,43], and the immuno-targeting efficiency depends on the antibody density on the surface [44]. Thus, highly efficient targeting and a relatively low level of RES uptake of immunoliposomes are apparently mutually exclusive.

To study whether immunoliposomes injected intravenously can extravasate into solid tumors and bind to tumor cells, we used the monoclonal antibody 21B2, specific for the human carcinoembryonic antigen (CEA), and mice bearing CEA-positive human gastric cancer strain MKN-45 [45]. 21B2 was isolated from BALB/c mice after immunization with human CEA antigen, purified from CEA-producing human gastric cancer strain MKN-45 cells. Fab' fragments of 21B2 were prepared by pepsin digestion of the antibody and 2-aminoethanethiol reduction of the $F(ab')_2$ fragments. A series of PEG-immunoliposomes were designed to investigate the role of PEG molecules in immunoliposome binding to the target cells. We synthesized distearoyl-N-(3-carboxypropionoyl) polyethyleneglycol phosphatidylethanolamine (DSPE-PEG-COOH), and the dipalmitoyl phosphatidyl ethanolamine derivative of PEG (DPPE-PEG), for the preparation of IgG-PEG-immunoliposomes and Fab'-PEG-immunoliposomes, respectively [46,47]. In *in vitro* binding assays, PEG-immunoliposomes conjugated with either IgG (whole antibody of 21B2) or the Fab' fragment of 21B2 readily bound to MKN-45 cells. These results revealed that free PEG (not linked to the antibody) in

Table 1
Liposomal drugs on the market.

Formulation	Drug	Product	Seller
Conventional liposome	Doxorubicin	Myocet	Elan
	Daunorubicin	DaunoXome	Gilead
	Cytarabine	DepoCyte	Skye Pharma/Enzon/ Mundipharma
	Vincristine	Marqibo	Hana Biosciences
PEG-liposome	Doxorubicin	Doxil/Caelyx	Alza/J&J/Schering-Plough
	Cisplatin	Lipoplatin	Regulon
	Belotecan	Camtobell(CK D602)	Alza/J&J

Table 2
Pharmacokinetic properties in human of free doxorubicin, conventional liposomal doxorubicin (Myocet) and PEG-liposomal doxorubicin (Doxil, Caelyx). Liposome diameter: 85 to 150 nm. Data normalisation using an average body surface area of 1.7 m^2 and an average body weight of 70 kg. Examples of representative studies: Hamilton et al., 2002; Gabizon et al., 2003; Mross et al. 2004.

	Free doxorubicin	Myocet conventional liposomal	Doxil/Caelyx PEG-liposome
Dose (mg/kg)	1.2	1.8	1.5
AUC (mg.h/L)	3.5	19.4	4082
Clearance (ml/h)	25300	9520	23
Vss (L)	365	139	3.0
Half-life (h)	0.06/10.4*	<1/52.6*	84

*Two elimination phases.

liposomes does not interfere sterically with antigen binding of the antibody or Fab' fragment.

The tissue distribution of IgG-PEG-immunoliposomes and Fab'-PEG-immunoliposomes was examined by inoculating CEA-positive human gastric cancer strain MKN-45 cells inoculated into BALB/c *nu/nu* mice. As shown in Fig. 2, PEG-Mal liposomes without the antibody showed prolonged residence in the circulation and low liver uptake, regardless of the presence of the terminal maleimidyl group. There were no marked differences in tissue distribution among liposomes containing DSPE-PEG(-OCH_3), DSPE-PEG-COOH and DPPE-PEG-Mal. IgG-PEG-immunoliposomes, bearing approximately 51 molecules of 21B2 (whole antibody) per liposome, were rapidly cleared from the blood and were found entirely in the liver. In contrast, Fab'-PEG-immunoliposomes, bearing approximately 517 Fab' molecules of 21B2 per liposome, were retained longer in the circulation, with a concomitant decrease in the liver uptake compared with IgG-PEG-immunoliposomes. These results indicate that the linkage of whole 21B2 antibodies to the PEG termini enhances RES uptake via the Fc receptor-mediated mechanism [42,43]. To overcome this problem, it is necessary to use the Fab' fragment. In the case of Fab'-PEG-immunoliposomes, the absence of the Fc portion and the presence of free PEG-Mal (not linked to the Fab' fragment) may both play a role in prolonging the circulation of the liposomes. Thus, the Fab' fragment is much better than whole IgG in terms of designing PEG-immunoliposomes with prolonged circulation. Further, the usage of the Fab' fragment should greatly reduce the antigenicity.

We next investigated whether Fab'-PEG-immunoliposomes could extravasate into solid tumor tissue and bind to tumor cells. Fig. 2 shows the accumulation of Fab'-PEG-immunoliposomes, IgG-PEG-immunoliposomes and comparable PEG-liposomes, with an average diameter of 100-130 nm, in MKN-45 solid tumors 24 h after injection in mice. Relatively high accumulation was obtained with PEG-COOH liposomes, PEG-Mal liposomes and Fab'-PEG-immunoliposomes. These results were clearly correlated to their prolonged circulation time. The accumulation rate of Fab'-PEG-immunoliposomes was 2-fold higher than that of IgG-PEG-immunoliposomes or bare liposomes, and equal to that of PEG-Mal or PEG-COOH liposomes. The permeability of tumor vasculature is generally increased compared to normal tissue, so the smaller Fab'-PEG-immunoliposomes with its prolonged circulation time could extravasate through the leaky endothelium by passive convective transport. Ligand-directed targeting by Fab'-recognition is rather weak. On the other hand, IgG-PEG-immunoliposomes exhibited a short circulation time due to high liver uptake, so they lack both sufficient concentration and residence time to allow extravasation through the leaky endothelium. Though there were no differences in accumulation into solid tumors between Fab'-PEG-immunoliposomes and PEG-liposomes without antibodies, only Fab'-PEG-immunoliposomes stand a better chance of binding to the surface of MKN-45 cells. This is important for the extravasated Fab'-PEG-immunoliposomes, because Fab'-PEG-immunoliposomes can bind readily with MKN-45 cells in *in vitro* binding assays. This delivery system is particularly important for the endocytotic internalization of bioactive materials. However, in some other cases, the liposome internalization seems not to be important. It was shown in Sapra and Allen [48] that PEG-liposomes loaded with vincristin or doxorubicin and modified with antibodies against internalizing CD19 antigen or noninternalizing CD20 antigen demonstrate therapeutic effect which dependent more on the type of drugs used than on its ability to be internalized. The cytotoxicity of target liposomes depended also on the rate of drug release from the liposomes.

5. Liposomal drugs for intracellular targeting delivery to solid tumors based on EPR effects

Tumor-specific targeting therapies have been advocated as a means of increasing the therapeutic effect and decreasing the side effects of drugs. Intracellular targeting using iron-saturated transferrin (TF) as a ligand for receptor-mediated endocytosis has attracted attention. TF is a glycoprotein that transports ferric ions in the body, and TF receptor is internalized into cells by endocytosis through the binding of TF. This receptor-mediated endocytosis is a normal physiological process by which iron is delivered into cells [49,50].

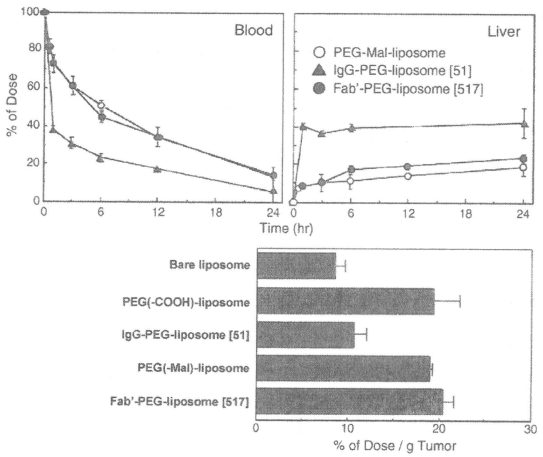

Fig. 2. Time course of blood residence, liver uptake and tumor accumulation of PEG-liposomes, IgG-PEG-liposome [51] or Fab'-PEG-liposome [517] in MKN-45- bearing BALB/c nu/nu mice. Two million MKN-45 cells were inoculated into the backs of female BALB/c nu/nu mice. The numbers in parentheses represent the average numbers of whole antibodies of 21B2 or Fab' molecules of 21B2 per liposome.

After binding of TF to the receptors on the cell surface, the TF-receptor complexes are internalized to form endosomes through clathrin-coated vesicles. After internalization, iron-loaded TF releases its iron due to the low endosomal pH, while iron-free TF remains bound to the receptor. These complexes are sorted into exocytic vesicles for delivery back to the cell surface and iron-free TF is released. The entire TF cycle takes only 4-5 min, with a mean transit time of about 10 min, and avoids the lysosomal compartment. As the TF receptor concentration on the cell membrane is reported to be higher in various types of tumor cells than in normal cells, correlating with the aggressive or proliferate ability of cells [50,51]. TF receptor is considered to be useful as a potential target for drug delivery into tumor cells.

We have explored the possibility of using TF for developing an intracellular drug delivery system [52]. TF was coupled to the distal termini of the PEG chains to prepare TF-PEG-liposome, as previously described [52]. TF-PEG-liposomes, bearing approximately 25 TF molecules per liposome, readily bound to mouse Colon 26 cells *in vitro*, and were internalized by receptor-mediated endocytosis.

TF-PEG-liposomes exhibited interesting properties with regards to biodistribution, tumor accumulation and internalization *in vivo*. As shown in Fig. 3, TF-PEG-liposomes had a prolonged circulation time and low RES uptake in Colon 26 tumor-bearing mice, resulting in enhanced extravasation of the liposomes into the solid tumor tissue. Coupling of TF molecules did not enhance RES uptake of liposomes, presumably because TF is an abundant serum glycoprotein (2.5 mg/ml) that transports ferric ion in the body. Electron microscopy studies in Colon 26 tumor-bearing mice revealed that the extravasated TF-PEG-liposomes were internalized into tumor cells by receptor-mediated endocytosis. TF-PEG-liposomes were taken up into endosomal-like intracellular vesicles, as visualized by transmission electron microscopy (data not shown) and maintained a high drug level in the tumor for over 60 h after injection (Figs. 3 and 4). This high retention indicates cellular uptake of the extravasated TF-PEG-liposomes by TF-receptor-mediated endocytosis. Thus, TF-PEG-liposomes are potential tools for *in vivo* cytosolic delivery of anticancer drugs in cancer chemotherapy, as well as of nucleic acids in gene therapy.

We and Liu et al. previously demonstrated that a relatively high level of tumor accumulation of PEG-liposomes correlated very well with both a small size (less than 200 nm in diameter) and a relatively high concentration of liposomes in the blood [9,25,52]. Though there were no marked differences in accumulation in solid tumors between TF-PEG-liposomes and PEG-liposomes averaging 120 nm in diameter, only TF-PEG-liposomes bound specifically to tumor cells. Notably, the residence time of extravasated TF-PEG-liposomes in tumor tissues was much longer than that of PEG-liposomes (Fig. 4). TF-PEG-liposomes escaped from leaky endothelial barriers and extravasated into the extravascular and interstitial space among tumor cells.

Huwyler et al. pointed out in their review [34] that the transferrin receptor (which has a dissociation constant of 5.6 nM) is saturated *in vivo* by the μM endogenous plasma transferrin concentrations [53]. This strong competition with endogenous transferrin leads to poor *in vivo* receptor targeting after intravenous injection. However, *in vivo* data (Figs. 3 and 4) of TF-PEG-liposomes showed that this strong competition tends to inhibit the binding of TF-PEG-liposomes to normal cells after intravenous injection. Consequently, TF-PEG-liposomes remain in blood circulation for a long period and extravasate into the extravascular of tumor tissue by the EPR effect as PEG-liposomes. The decreased flow in the interstitial space among tumor cells provides TF-PEG-liposomes with a greater chance to bind to the TF receptors on the surface of the tumor cells, even in the presence of endogenous plasma transferrin.

6. Intracellular targeting of sodium mercaptoundecahydrododecaborate (^{10}BSH) to solid tumors by transferrin-PEG liposomes, for boron neutron-capture therapy (BNCT) [54]

BNCT is aimed at inhibiting the growth of various cancers [55]. The stable isotope of boron, ^{10}B, interacts with low energy (thermal) neutrons to produce highly energetic, short-range disintegration products. The resultant lithium ions and particles are high linear energy transfer particles with relatively high biological efficiency. These particles (α and ^{7}Li) destroy cells within a radius about 10 μm from the site of the capture reaction. It is theoretically possible to kill tumor cells without affecting adjacent healthy cells if ^{10}B atoms can be selectively accumulated in the interstitial space of tumor tissue and/or the intracellular space between tumor cells. The neutron component of this therapy by itself would have little effect on tumor or normal tissue, and thermal neutrons (<0.4 eV) have insufficient energy to damage tissue. The preferential localization of a ^{10}B compound in a tumor cell, followed by neutron irradiation, results in the destruction of the tumor cell without damage to surrounding normal cells [56]. When ^{10}B is present on the cell surfaces of a tissue, its cell-killing effect is greatly reduced compared to when it is accumulated inside the cell. Thus, successful treatment of cancer by BNCT requires the selective delivery of relatively large amounts of ^{10}B compounds to malignant cells. The estimated boron concentration required for effective therapy is in the range of 20-30 μg ^{10}B per g of tissue [57]. At the same time, the boron concentration in the surrounding normal tissue should be kept low to minimize damage to the normal tissue.

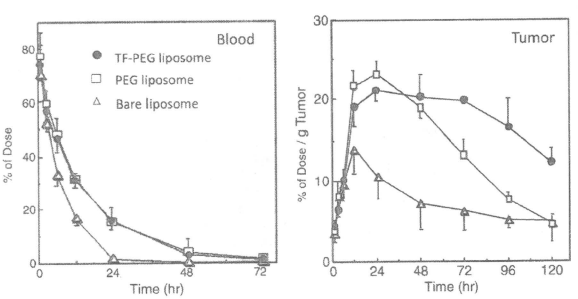

Fig. 3. Time courses of blood residence and tumor accumulation of TF-PEGliposomes, with an average of 25 TF molecules per liposome, after intravenous injection. Liposomes (100-130 nm average diameter) labeled with ^{3}H-CHE were injected into Colon 26 tumor-bearing mice at a dose of 500 μg lipid. Data are expressed as mean ± S.D. (n = 3-5).

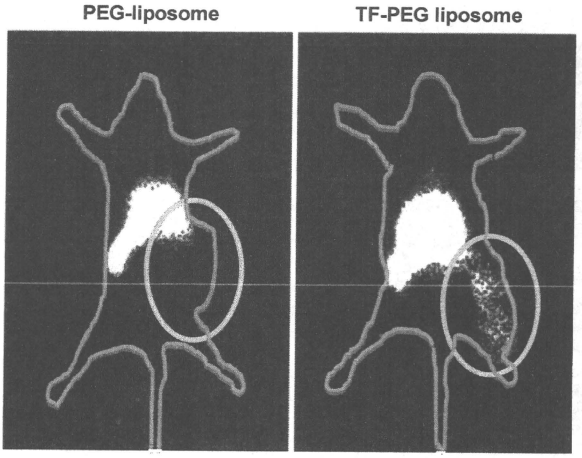

Fig. 4. Gamma ray imaging of TF-PEG Liposome in Colon 26 solid tumor tissue *in vivo*. TF-PEG-liposomes of 132 ± 38 nm mean diameter, entrapping ^{111}In-DTPA and coupling an average of 25 TF molecules per liposome, were injected into mice *via* the tail vein, and gamma ray imaging were taken 60 hr after administration.

When TF-PEG liposomes with an average diameter of 100-200 nm were injected at a dose of 35 mg/kg ^{10}B, we observed prolonged circulation and low uptake by the RES in Colon 26 tumor-bearing mice, resulting in enhanced accumulation of ^{10}B into the solid tumor tissue (e.g., 35.5 μg/g) (Figs. 5 and 6). The most likely mechanism for this accumulation is the increased blood circulation time of liposomes and the leaky structure of the microvasculature in solid tumor tissue (the EPR effect). The accumulation of TF-PEG-liposomes and PEG-liposomes in tumor tissue is directly proportional to the AUC_{plasma} of the plasma clearance. TF-PEG liposomes produced high ^{10}B levels in the tumor, with concentrations over 30 μg/g for at least 72 h after injection. This high retention of ^{10}B in tumor tissue indicates that binding and concomitant cellular uptake of the extravasated TF-PEG liposomes occurs by TF receptor and receptor-mediated endocytosis, respectively. On the other hand, the level of ^{10}B in plasma decreased, resulting in a tumor/plasma ^{10}B ratio of 6.0 at 72 h after injection. Notably, the level of ^{10}B in plasma was very low at 72 h after injection of TF-PEG liposomes, from the viewpoint of preventing damage to the endothelium. Such damage can be serious if reactor exposures take place when plasma boron levels are high [32]. The long retention of TF-PEG liposomes in tumor tissue provides sufficient time for the plasma ^{10}B concentration to fall substantially, resulting in a tumor/plasma ratio of 6.0 at 72 h after injection. The level of ^{10}B in the liver was also low at this time. These characteristics are therapeutically favorable. Thus, ≥ 72 h after injection of TF-PEG liposomes was selected as a suitable time point for BNCT treatment.

Administration of BSH encapsulated in TF-PEG liposomes at a dose of 5 - 35 mg/kg ^{10}B and irradiation with 2×10^{12} neutrons/cm^2 for 37 min suppressed tumor growth and improved long-term survival compared with PEG liposomes, bare liposomes and free BSH. Thus, intravenous injection of TF-PEG liposomes can increase the tumor retention of ^{10}B atoms, which were introduced by receptor-mediated

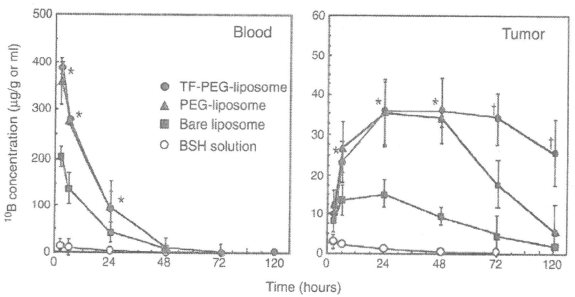

Fig. 5. Time courses of blood residence and tumor accumulation of ^{10}B delivered by each kind of liposome encapsulating BSH, and by BSH solution, in Colon 26 tumorbearing mice. Two hundred to 300 μl of BSH-TF-PEG liposomes, BSH-PEG liposomes, BSH bare liposomes or BSH solution was injected into tumor-bearing mice *via* the tail vein at a dose of 35 mg ^{10}B/kg. TF-PEG liposomes, with an average of 20 TF molecules per liposome, were used. Data are expressed as mean ± SD (n = 5).

Author personal copy

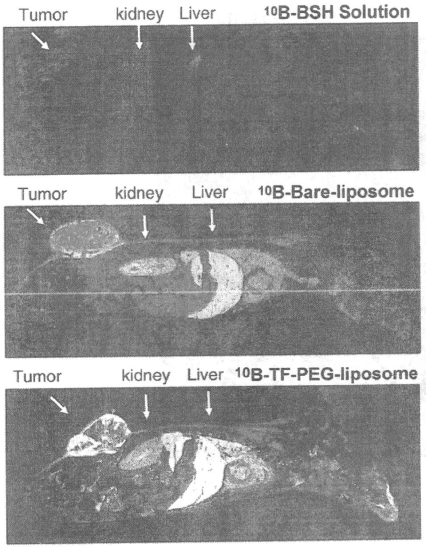

Fig. 6. Neutron capture autoradiography images of the wholebody section of Colon 26 bearing mice at 48 hr after iv injection.

endocytosis of liposomes after binding, causing tumor growth suppression *in vivo* upon thermal neutron irradiation. These results suggest that TF-PEG-liposomes are a suitable intracellular targeting carrier in BNCT therapy for cancer.

7. Intracellular targeting of oxaliplatin to solid tumors by transferrin-PEG liposomes

Oxaliplatin (trans-l-diaminocyclohexane oxalatoplatinum, L-OHP) is a novel cisplatin derivative that can reduce the side effects of cisplatin, such as toxicity to the kidneys. However, L-OHP is effective only when combined with 5-fluorouracil (5-FU) and leucovorin. The relatively low anti-tumor index of L-OHP alone is because only low levels accumulate in tumor tissues due to high partitioning to erythrocytes *in vivo*. A successful outcome of cancer therapy using L-OHP requires the selective delivery of a relatively high concentration of the drug to tumors.

We examined the tumor-selective delivery of L-OHP using TF-PEG-liposomes [58]. Fig. 7A shows the time course of plasma clearance after i.v. injection of L-OHP in solution and liposomal L-OHP. L-OHP in solution was rapidly cleared from the blood circulation whereas the circulation of L-OHP encapsulated within liposomes was increased. The blood concentrations of L-OHP encapsulated within PEG- and TF-PEG-liposomes were much higher than that of L-OHP encapsulated within Bare liposomes. Fig. 7B shows the biodistribution of L-OHP in solution and of L-OHP encapsulated within various liposomes at 6 h after intravenous (i.v.) injection. The results show that very little L-OHP was distributed to the major tissues in mice. In contrast, the distribution of L-OHP encapsulated in PEG- and TF-PEG-liposomes to the liver and spleen differed, but far less of both was distributed to these tissues compared with Bare liposomes. These results indicate that the PEG layer prolonged the systemic circulation of liposomes after i.v. injection. Thus, the conjugation of TF to the PEG termini did not alter the RES uptake of PEG-liposomes, presumably because TF is a blood glycoprotein.

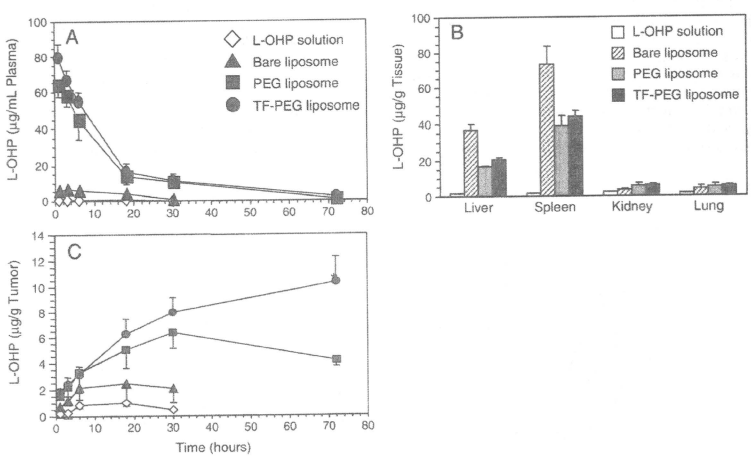

Fig. 7. Plasma clearance (A), biodistribution (B) and tumor accumulation of L-OHP solution or liposomal L-OHP in Colon 26-bearing mice. L-OHP in solution or encapsulated within Bare, PEG- or TF-PEG-liposomes (L-OHP: 5 mg/kg) was injected via tail veins of Colon 26-bearing mice. A: At various times thereafter, blood samples were collected using glass capillaries from veins of fundus oculi. Plasma L-OHP levels were measured by MIP-MS. B: Six hours later, mice were sacrificed and liver, spleen, kidneys and lungs were collected. C: At various times thereafter, tumor tissue was collected from the mice. Concentrations of L-OHP in tissue samples were measured by MIP-MS.

Fig. 7C shows the time course of L-OHP in Colon 26 solid tumor tissue after i.v. injection of L-OHP in solution or encapsulated within bare, PEG- or TF-PEG-liposomes. The concentrations of L-OHP in tumor tissue at 18 h after i.v. injection of L-OHP in solution and in bare liposomes were 0.98 and 2.1 μg/g tumor, respectively, and did not increase thereafter. The concentrations of L-OHP encapsulated within PEG- and TF-PEG-liposomes in tumor tissue were higher than that of L-OHP in solution and in bare liposomes. The L-OHP concentration in tumor tissue decreased 30 h after i.v. injection of L-OHP encapsulated within PEG-liposomes. Interestingly, the profiles of L-OHP encapsulated within TF-PEG- and PEG-liposomes in tumor tissues differed. The concentration of L-OHP encapsulated within TF-PEG-liposomes continued to increase until 72 h after i.v. injection, and a high L-OHP concentration was maintained in the tumor for a longer period. Tumor growth was somewhat suppressed to a similar extent by L-OHP in solution and encapsulated within bare or PEG-liposomes, but was significantly suppressed by L-OHP encapsulated within TF-PEG-liposomes (Fig. 8).

Effective anti-tumor therapy by L-OHP requires its internalization into the cytoplasm of tumor cells because this drug works by inhibiting DNA synthesis and transcription by forming DNA adducts [59]. The therapeutic effects of PEG-liposomes and L-OHP in solution were similar. It therefore appears that PEG-liposomes can deliver L-OHP to tumor tissue through the EPR effect, but are not effectively internalized into the cytoplasm. In contrast, TF-PEG-liposomes appear to deliver L-OHP into the cytoplasm of tumor cells via TF receptor-mediated endocytosis after extravasation by the EPR effect.

Actually, the retention time of PEG- and TF-PEG-liposomes in tumor tissues differed, despite their prolonged circulation in the blood. These results supported the notion that TF-PEG-liposomes deliver L-OHP to the surface and the interior of tumor cells. Prolonged circulation of TF-PEG-liposomes in the blood increased the amount of time that various tissues, including tumors, were exposed to L-OHP. In addition, TF receptors were also expressed on normal cells. We considered the possibility of a concomitant increase in the incidence of acute toxicity after a single L-OHP i.v. injection. However, blood biochemistry tests revealed that the tested parameters remained within their normal range. These findings indicated that L-OHP encapsulated within TF-PEG-liposomes did not induce any significant acute toxicity in the presence of increased distribution to the liver compared with L-OHP in solution. We also examined the biodistribution of L-OHP encapsulated within TF-PEG-liposomes in other experiments, and found that the concentration of L-OHP in the brain was very low (about 0.06 μg/g tissue) at 72 h after i.v. injection of the liposomes. Additionally, abnormal behavior was not observed in the mice. Therefore, it was thought that significant side effects were not induced in the brain. Furthermore, we did not observe any remarkable decrease in body weight after two i.v. injections of liposomal L-OHP. These results indicated that the frequency of serious side effects was minimal. Although L-OHP is a useful anti-tumor drug, it is rapidly cleared from the blood. We addressed this issue using TF-PEG-liposomes as a carrier for L-OHP. In conclusion, TF-PEG-liposomes, which allow both passive and active targeting, are a potential carrier for *in vivo* cytoplasmic targeting of L-OHP in solid tumors over-expressing surface TF receptors.

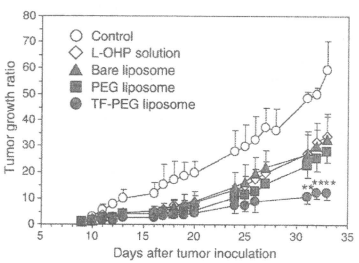

Fig. 8. Comparison of tumor growth suppression with L-OHP in solution and in liposomes in Colon 26-bearing mice. L-OHP solution or L-OHP encapsulated within Bare, PEG- or TF-PEG-liposomes (L-OHP: 5 mg/kg) was injected via tail veins of Colon 26-bearing mice on days 9 and 12 after tumor cell inoculation. Data are shown as means and standard deviation (n = 4). **P < 0.01 (PEG-liposomes vs. TF-PEG-liposomes).

Based on the above results, MBP-426 was developed by a Japanese venture company. Phase I clinical trials for solid tumors are finished [60] and phase IIa studies are ongoing. MBP-426 is a transferrin-conjugated liposome formulation of oxaliplatin (L-OHP). MBP-426 improves the safety and efficacy of oxaliplatin by both passive targeting by prolonged circulation and active targeting by TF.

8. Conclusion

There are several clear aims when using ligand-mediated tumor targeting of drug-loaded nanocarriers compared to more traditional dosage forms [61]. Ideally, drugs in nanocarriers should not only accumulate in the interstitial space inside tumors but also be internalized by the target cells creating high intracellular drug concentration and allowing multidrug resistance to be bypassed. To achieve these goals, certain considerations should be taken into account: (1) a target should be identified which is present (over-expressed) on the surface of tumor cells in sufficient quantity providing good opportunity for the targeted liposomes to firmly bind with cancer cells; (2) the specific ligand should be attached to the surface of the drug-loaded nanocarriers in a way which does not affected its specific binding properties and long circulating activity in blood; (3) the targeting ligand is internalizable and facilitates the internalization of the carrier and carrier-incorporated anti-cancer drug; (4) drug release from carrier inside the tumor or inside the tumor cell should deliver the therapeutic concentration of the drug and maintain it for a reasonable period of time.

TF is a glycoprotein that transports ferric ions in the body, and TF receptor is internalized into cells by endocytosis through the binding of TF. TF-PEG-liposomes can stay in blood circulation for a long time and extravasate into the extravascular of tumor tissue by the EPR effect as PEG-liposomes. TF-PEG-liposomes can deliver incorporated anti-cancer drug into the cytoplasm of tumor cells via TF receptor-mediated endocytosis after extravasation by the EPR effect. Thus, TF-PEG-liposomes show promise in the clinical environment as a carrier for chemotherapy agents against various types of tumors that overexpress TF receptors.

References

[1] G. Gregoriadis, Liposome Technology, Third Ed.Informa, New York, 2007.
[2] V. Weissig, Liposomes, Springer, New York, 2009.
[3] D.C. Drummond, O. Meyer, K. Hong, D.B. Kirpotin, D. Papahadjopoulos, Optimizing liposomes for delivery of chemotherapeutic agents to solid tumors, Pharmacol. Rev. 51 (1999) 691–743.
[4] T.M. Allen, C. Hansen, Pharmacokinetics of stealth versus conventional liposomes: effect of dose, Biochim. Biophys. Acta 1068 (1991) 133–141.
[5] M.S. Ewer, F.J. Martin, C. Henderson, C.L. Shapiro, R.S. Benjamin, A.A. Gabizon, Cardiac safety of liposomal anthracyclines, Semin. Oncol. 31 (2004) 161–181.
[6] M.M. Frank, The reticuloendothelial system and bloodstream clearance, J. Lab. Clin. Med. 122 (1993) 487–488.
[7] T. Daemen, G. Hofstede, M.T. Ten Kate, I.A. Bakker-Woudenberg, G.L. Scherphof, Liposomal doxorubicin induced toxicity: depletion and impairment of phagocytic activity of liver macrophages, Int. J. Cancer 61 (1995) 716–721.
[8] K. Maruyama, T. Yuda, A. Okamoto, S. Kojima, A. Suginaka, M. Iwatsuru, Prolonged circulation time in vivo of large unilamellar liposomes composed of distearoyl phosphatidylcholine and cholesterol containing amphipathic poly(ethylene glycol), Biochim. Biophys. Acta 1128 (1992) 4–9.
[9] D. Liu, A. Mori, L. Huang, Role of liposome size and RES blockade in controlling biodistribution and tumor uptake of GM1-containing liposomes, Biochim. Biophys. Acta 1104 (1992) 95–101.

[10] R.K. Jain. Transport of molecules across tumor vasculature. Cancer Metastasis Rev. 6 (1987) 559.
[11] H.K. Dvorak, J.A. Nagy, J.T. Dvorak, A.M. Dvorak. Identification and characterization of the blood vessels of solid tumors that are leaky to circulating macromolecules. Am. J. Phathol. 133 (1988) 95–109.
[12] Y. Matsumura, H. Maeda, A new concept for macromolecular therapeutics in cancer chemotherapy: mechanism of tumoritropic accumulation of proteins and the antitumor agent smancs, Cancer Res. 46 (1986) 6387–6392.
[13] H. Maeda, The tumor blood vessel as an ideal target for macromolecular anticancer agents, J. Control. Release 19 (1992) 315–324.
[14] H. Maeda, L.W. Seymour, Y. Miyamoto, Conjugation of anticancer agents and polymers: advantages of macromolecular therapeutics in vivo, Bioconjug. Chem. 3 (1992) 351–362.
[15] A. Klibanov, K. Maruyama, V.P. Torchilin, L. Huang, Amphipathic polyethyleneglycols effectively prolong the circulation time of liposomes, FEBS Lett. 268 (1990) 235–237.
[16] G. Blume, C. Cevc, Liposomes for the sustained drug release in vivo, Biochim. Biophys. Acta 1029 (1990) 91–97.
[17] T.M. Allen, C. Hansen, F. Martin, C. Redemann, A.Y. Young, Liposomes containing synthetic lipid derivatives of poly(ethylene glycol) show prolonged circulation half-lives in vivo, Biochim. Biophys. Acta 1066 (1991) 29–36.
[18] K. Maruyama, T. Yuda, A. Okamoto, S. Kojima, A. Suginaka, M. Iwatsuru, Prolonged circulation time in vivo of large unilamellar liposomes composed of distearoyl phosphatidylcholine and cholesterol containing amphipathic poly(ethylene glycol), Biochim. Biophys. Acta 1128 (1992) 44–49.
[19] C. Allen, N. Dos Santos, R. Gallagher, G.N. Chiu, Y. Shu, W.M. Li, S.A. Johnstone, A.S. Janoff, L.D. Mayer, M.S. Webb, M.B. Bally, Controlling the physical behavior and biological performance of liposome formulations through use of surface grafted poly(ethylene glycol), Biosci. Rep. 22 (2002) 225–250.
[20] Y.S. Park, K. Maruyama, L. Huang, Some negatively charged phospholipid derivatives prolong the liposome circulation in vivo, Biochim. Biophys. Acta 1108 (1992) 257–260.
[21] K. Maruyama, S. Okuizumi, O. Ishida, H. Yamauchi, H. Kikuchi, M. Iwatsuru, Phosphatidyl polyglycerols prolong liposome circulation in vivo, Int. J. Pharm. 111 (1994) 103–107.
[22] Y. Sadzuka, A. Nakade, R. Hirama, A. Miyagishima, Y. Nozawa, S. Hirota, T. Sonobe, Effects of mixed polyethyleneglycol modification on fixed aqueous layer thickness and antitumor activity of doxorubicin containing liposome, Int. J. Pharm. 238 (2002) 171–180.
[23] S.M. Moghimi, H.M. Patel, Opsonophagocytosis of liposomes by peritoneal macrophages and bone marrow reticuloendothelial cells, Biochim. Biophys. Acta 1135 (1992) 269–274.
[24] S. Unezaki, K. Maruyama, O. Ishida, A. Suginaka, J. Hosoda, M. Iwatsuru, Enhanced tumor targeting and improved antitumor activity of doxorubicin by long-circulating liposomes containing amphipathic poly(ethylene glycol), Int. J. Pharm. 126 (1995) 41–48.
[25] S. Unezaki, K. Maruyama, J. Hosoda, I. Nagae, Y. Koyanagi, M. Nakata Test, article sample title placed here, Int. J. Pharm. 144 (1996) 11–17.
[26] S.K. Huang, K.D. Lee, K. Hong, D.S. Friend, D. Papahadjopoulos, Microscopic localization of sterically stabilized liposomes in colon carcinoma-bearing mice, Cancer Res. 52 (1992) 5135–5143.
[27] F. Yuan, M. Dellian, D. Fukumura, M. Leunig, D.A. Berk, V.P. Torchilin, R.K. Jain, Vascular permeability in a human tumor xenograft: molecular size dependence and cutoff size, Cancer Res. 55 (1995) 3752–3756.
[28] A.A. Gabizon, Pegylated liposomal doxorubicin: metamorphosis of an old drug into a new form of chemotherapy, Cancer Invest. 19 (2001) 424–436.
[29] J.W. Park, C.C. Benz, F.J. Martin, Future directions of liposomeand immunoliposome-based cancer therapeutics, Semin. Oncol. 31 (2004) 196–205.
[30] R.D. Hofheinz, S.U. Gnad-Vogt, U. Beyer, Liposomal encapsulated anti-cancer drugs, Anticancer Drugs 16 (2005) 691–707.
[31] F. Martin, T. Boulikas, The challenge of liposomes in gene therapy, Gene Ther. Mol. Biol. 1 (1998) 173–214.
[32] G.P. Stathopoulos, T. Boulikas, M. Vougiouka, G. Deliconstantinos, S. Rigatos, E. Darli, V. Viliotou, J.G. Stathopoulos, Pharmacokinetics and adverse reactions of a new liposomal cisplatin (Lipoplatin™): Phase I study, Oncol. Rep. 13 (2005) 589–595.
[33] D.N. Waterhouse, P.G. Tardi, L.D. Mayer, A comparison of liposomal formulations of doxorubicin with drug administered in free form: changing toxicity profiles, Drug Saf. 24 (2001) 903–920.
[34] J. Huwyler, J. Drewe, S. Krähenbuhl, Tumor targeting using liposomal antineoplastic drugs, Int. J. Nanomed. 3 (2008) 21–29.
[35] A. Hamilton, L. Biganzoli, R. Coleman, A phase I clinical and pharmacokinetic study of polyethylene glycol liposomal doxorubicin (Caelyx, Doxil) at a 6-week interval in patients with metastatic breast cancer, EORTC Ann. Oncol. 13 (2002) 910–918.
[36] A. Gabizon, H. Shmeeda, Y. Barenholz, Pharmacokinetics of pegylated liposomal Doxorubicin: review of animal and human studies, Clin. Pharmacokinet. 42 (2003) 419–436.
[37] K. Mross, B. Niemann, U. Massing, Pharmacokinetics of liposomal doxorubicin (TLC-D99; Myocet) in patients with solid tumors: an open-label, single-dose study, Cancer Chemother. Pharmacol. 54 (2004) 514–524.
[38] M.S. Ewer, F.J. Martin, C. Henderson, Cardiac safety of liposomal anthracyclines, Semin. Oncol. 31 (2004) 161–181.
[39] A.A. Gabizon, H. Shmeeda, S. Zalipsky, Pros and cons of the liposome platform in cancer drug targeting, J. Liposome Res. 16 (2006) 175–183.
[40] T.M. Allen, Liposomal Drug Formulations, Drugs 56 (1998) 747–756.
[41] K. Maruyama, O. Ishida, T. Takizawa, K. Moribe, Possibility of active targeting to tumor tissues with liposomes, Adv. Drug Deliv. Rev. 40 (1999) 89–102.
[42] D. Aragnol, L.D. Leserman, Immune clearance of liposomes inhibited by an anti-Fc receptor antibody in vivo, Proc. Natl Acad. Sci. USA 83 (1986) 2699–2703.
[43] J.T.P. Derksen, H.W.M. Marselt, G.L. Scherphof, Uptake and processing of immunoglobulin-coated liposomes by subpopulation of rat liver macrophages, Biochim. Biophys. Acta 971 (1988) 127–136.
[44] K. Maruyama, E. Holmberg, S.J. Kennel, A. Klibanov, V.P. Torchilin, L. Huang, Characterization of in vivo immunoliposome targeting to pulmonary endothelium, J. Pharm. Sci. 79 (1990) 978–984.
[45] I. Uyama, K. Kunai, T. Yasuda, T. Tagawa, K. Ishibiki, M. Kitajima, T. Tadakuma, Improvement of therapeutic effect by using Fab' fragment in the treatment of carcinoem bryonic antigen-positive human solid tumors with adriamycin-entrapped immunoliposomes, Jpn J. Cancer Res. 85 (1994) 434–440.
[46] K. Maruyama, T. Takizawa, T. Yuda, S.J. Kennel, L. Huang, M. Iwatsuru, Targetability of novel immunoliposomes modified with amphipathic polyethyleneglycols conjugated at their distal terminals to monoclonal antibodies, Biochim. Biophys. Acta 1234 (1995) 74–80.
[47] K. Maruyama, N. Takahashi, T. Tagawa, K. Nagaike, M. Iwatsuru, Immunoliposomes bearing polyethyleneglycol -coupled Fab' fragment show prolonged circulation time and high extravasation into target solid tumors in vivo, FEBS Lett. 413 (1997) 177–180.
[48] P. Sapra, T.M. Allen, Improved outcom when B-cell lymphoma is treated with combinations of immunoliposomal anticancer drugs targeted to both the CD19 and CD20 epitopes, Clin. Cancer Res. 10 (2004) 2530–2537.
[49] K. Thorstein, I. Romslo, The transferrin receptor: Its diagnostic value and its potential as therapeutic target, Scan. J. Clin. Lab. Invest. Suppl. 215 (1993) 113–120.
[50] E. Wagner, D. Curiel, M. Cotton, Delivery of drugs, proteins and genes into cells using transferrin as a ligand for receptor-mediated endocytosis. Adv. Drug Deliv. Rev. 14 (1994) 113–135.
[51] T. Miyamoto, N. Tanaka, Y. Eishi, T. Amagasa, Transferrin receptor in oral tumors, Int. J. Oral Maxillofac. Surg. 23 (1994) 430–433.
[52] O. Ishida, K. Maruyama, K. Sasaki, M. Iwatsuru, Size-dependent extravasation and interstitial localization of polyethyleneglycol liposomes in solid tumor-bearing mice, Int. J. Pharm. 190 (1999) 49–56.
[53] W.M. Pardridge, Brain drug delivery and blood-brain barrier transport, Drug Deliv. 1 (1993) 83–101.
[54] K. Maruyama, H. Yanagie, O. Ishida, S. Kasaoka, T. Takizawa, N. Utoguchi, A. Shinohara, M. Chiba, H. Kobayashi, M. Iwatsuru, M. Eriguchi, Intracellular targeting of sodium mercaptoundecahydrododecaborate (BSH) to solid tumors by transferrin-PEG liposomes, for boron neutron-capture therapy (BNCT), J. Control. Release 98 (2004) 195–207.
[55] M.F. Hawthorne, The role of chemistry in the development of boron neutron capture therapy of cancer, Angew. Chem. Int. Ed Engl. 32 (1993) 950–984.
[56] R.F. Barth, A.H. Soloway, R.G. Fairchild, Boron neutron capture therapy for cancer, Cancer Res. 50 (1990) 1061–1070.
[57] R.F. Barth, A.H. Soloway, R.G. Fairchild, R.M. Brugger, Boron neutron capture therapy for cancer, Cancer 70 (1992) 2995–3007.
[58] R. Suzuki, T. Takizawa, Y. Kuwata, M. Mutoh, N. Ishiguro, N. Utoguchi, A. Shinohara, M. Eriguchi, H. Yanagie, K. Maruyama, Effective anti-tumor activity of Oxaliplatin encapsulated in transferrin-PEG-liposome, Int. J. Pharm. 346 (2008) 143–150.
[59] L. Pendyala, Y. Kidani, R. Perez, J. Wilkes, R.J. Bernacki, P.J. Creaven, Cytotoxicity, cellular accumulation and DNA binding of oxaliplatin isomers. Cancer Lett. 97 (1995) 177–184.
[60] K.K. Sankhala, A.C. Mita, R. Adinin, L. Wood, M. Beeram, S. Bullock, N. Yamagata, K. Matsuno, T. Fujisawa, A. Phan, A phase I pharmacokinetic (PK) study of MBP-426, a novel liposome encapsulated oxaliplatin, J. Clin. Oncol. 27 (15 s) (2009) 2535.
[61] V.P. Torchilin, Passive and active drug targeting: drug delivery to tumors as an example, in: M. Schafer-Korting (Ed.), Handbook of Experimental Pharmacology, 197, Springer-Verlag, Berlin, 2010, pp. 4–36.

Published OnlineFirst on July 14, 2010 as 10.1158/0008-5472.CAN-10-0184

Molecular and Cellular Pathobiology

Cancer Research

Circadian Rhythm of Transferrin Receptor 1 Gene Expression Controlled by c-Myc in Colon Cancer–Bearing Mice

Fumiyasu Okazaki[1], Naoya Matsunaga[1], Hiroyuki Okazaki[1], Naoki Utoguchi[2], Ryo Suzuki[2], Kazuo Maruyama[2], Satoru Koyanagi[1], and Shigehiro Ohdo[1]

Abstract

The abundance of cell surface levels of transferrin receptor 1 (TfR1), which regulates the uptake of iron-bound transferring, correlates with the rate of cell proliferation. Because TfR1 expression is higher in cancer cells than in normal cells, it offers a target for cancer therapy. In this study, we found that the expression of TfR1 in mouse colon cancer cells was affected by the circadian organization of the molecular clock. The core circadian oscillator is composed of an autoregulatory transcription-translation feedback loop, in which CLOCK and BMAL1 are positive regulators and the *Period* (*Per*), *Cryptochrome* (*Cry*), and *Dec* genes act as negative regulators. TfR1 in colon cancer–bearing mice exhibited a 24-hour rhythm in mRNA and protein levels. Luciferase reporter analysis and chromatin immunoprecipitation experiments suggested that the clock-controlled gene *c-MYC* rhythmically activated the transcription of the *TfR1* gene. Platinum incorporation into tumor DNA and the antitumor efficacy of transferrin-conjugated liposome-delivered oxaliplatin could be enhanced by drug administration at times when TfR1 expression increased. Our findings suggest that the 24-hour rhythm of TfR1 expression may form an important aspect of strategies for TfR1-targeted cancer therapy. *Cancer Res; 70(15); OF1–9. ©2010 AACR.*

Introduction

In mammals, the master pacemaker controlling the circadian rhythm is located in the suprachiasmatic nuclei of the hypothalamus (1). Regulation of circadian physiology relies on the interplay of interconnected transcription-translation feedback loops. The BMAL1/CLOCK complex activates clock-controlled genes, including *Per*, *Cry*, and *Dec*, the products of which act as repressors by interacting with BMAL1/CLOCK (2–5). This mechanism also regulates the 24-hour rhythm in output physiology through the periodic activation/repression of clock-controlled output genes in healthy peripheral tissue and tumor tissue (6, 7).

Transferrin receptor 1 (TfR1) is involved in the uptake of iron into cells through the binding and internalization of transferrin, and its regulation by intracellular iron levels has assisted in the elucidation of many important aspects of cellular iron homeostasis (8, 9). Iron is important for metabolism, respiration, and DNA synthesis. Thus, TfR1 is expressed not only in normal healthy cells but also in malignant tumor cells (8, 10). Recently, another TfR-like molecule named TfR2 has been recognized and investigated (11, 12), but the exact function of TfR2 remains unclear (8). It has been reported that the expression of TfR1 in mammary epithelial cells exhibits a significant 24-hour rhythm (13). Such rhythmic variation in TfR1 expression seems to affect its iron uptake function resulting in time-dependent changes in the internalization of iron-loaded Tf. However, it is not clear if the expression of TfR1 in colon cancer cells shows a significant 24-hour rhythm.

Many of the pharmacologic properties of conventional drugs can be improved through the use of an optimized drug delivery system (DDS), which includes particular carriers composed primarily of lipids and/or polymers (14). The high expression of TfR1 in tumor can potentially be used to deliver cytotoxic agents into malignant cells, including chemotherapeutic drugs, cytotoxic proteins (8), and Tf-coupled polyethylene glycol (Tf-PEG) liposomes were designed as intracellular targeting carriers for drugs by systemic administration. In fact, Tf-PEG liposomes encapsulating a platinum (Pt)-based anticancer drug, oxaliplatin, can increase its accumulation in tumor masses (15, 16). On the other hand, daily rhythmic variations in biological functions are thought to affect the efficacy and/or toxicity of drugs: a large number of drugs cannot be expected to have the same potency at different administration times (7, 17). However, it is unclear what influence the rhythmic expression of TfR1 has on the pharmacokinetics/pharmacodynamics of transferrin targeting liposomes.

Authors' Affiliations: [1]Department of Pharmaceutics, Graduate School of Pharmaceutical Sciences, Kyushu University, Fukuoka, Japan and [2]Department of Pharmaceutics, Teikyo University, Sagamiko, Sagamihara, Japan

Note: Supplementary data for this article are available at Cancer Research Online (http://cancerres.aacrjournals.org/).

F. Okazaki, N. Matsunaga, and S. Ohdo contributed equally to this work.

Corresponding Author: Shigehiro Ohdo, Department of Pharmaceutics, Graduate School of Pharmaceutical Sciences, Kyushu University, Fukuoka, 812-8582, Japan. Phone: 81-92-642-6610; Fax: 81-92-642-6614; E-mail: ohdo@phar.kyushu-u.ac.jp.

doi: 10.1158/0008-5472.CAN-10-0184

©2010 American Association for Cancer Research.

In this study, we found that the circadian expression of *c-Myc*, which is controlled by the circadian clock, affects *TfR1* gene transcription in colon cancer cells. The levels of *TfR1* mRNA and protein exhibited a 24-hour oscillation in tumor cells implanted in mice. Thus, to evaluate the rhythmic function of TfR1 and the utility for TfR1-targeting cancer therapy, we investigated how the rhythmic variation in TfR1 production influenced the pharmacologic efficacy of TfR1-targeting liposomal DDS.

Materials and Methods

Animals and cells

Seven-week-old male BALB/c mice (Charles River Japan) were housed with lights on from 7:00 a.m. to 7:00 p.m. at a room temperature of 24 ± 1°C and a humidity of 60 ± 10% with food and water *ad libitum*. Colon 26 cells (Cell Resource Center for Biomedical Research, Tohoku University) were maintained in RPMI 1640 supplemented 10% fetal bovine serum (FBS) at 37°C in a humidified 5% CO_2 atmosphere. A 25-μL volume with 2×10^7 viable tumor cells was inoculated into the right hind footpad of each mouse. The tumor volume was estimated according to a formula that has been described previously (7). Tissue slices of the removed tumor masses were made, and the tumor tissue was confirmed histopathologically.

Experimental design

To assess the temporal expression profile of TfR1 in tumor cells, tumor masses were removed from individual tumor-bearing mice at six different time points (9:00 a.m., 1:00 p.m., 5:00 p.m., 9:00 p.m., 1:00 a.m., and 5:00 a.m.) 7 days after the implantation of tumor cells. The levels of *TfR1* protein and mRNA were measured by Western blotting analysis and quantitative reverse transcription-PCR (RT-PCR), respectively. To investigate how the rhythmic variation in *TfR1* expression occurs in tumor cells, the influence of CLOCK/BMAL1 and c-MYC on the transcriptional activity of the *TfR1* gene was assessed using luciferase reporter constructs containing wild-type E-box or mutated E-box of the mouse *TfR1* promoter, which was based on previous reports. To elucidate the role of c-MYC in the control of the rhythmic expression of *TfR1*, endogenous c-MYC in Colon 26 cells was downregulated by small interfering RNA (siRNA). The c-MYC–downregulated cells were treated with 50% FBS for 2 hours to synchronize their circadian clock, and the mRNA levels of *TfR1* were assessed at 44, 48, 52, 56, 60, 64, and 68 hours after 50% serum treatment. In the same manner as described above, the protein levels of c-MYC and CLOCK were assessed by Western blotting analysis. To explore the temporal binding of endogenous c-MYC and CLOCK to the E-box in the mouse *TfR1* gene, chromatin immunoprecipitation analysis was performed in individual tumor masses at 9:00 a.m. and 9:00 p.m. To investigate the function of the 24-hour oscillation of TfR1 expression, time-dependent changes in Pt internalization into tumor cells were assessed using Tf-coupled liposomes encapsulating oxaliplatin (Tf-NGPE L-OHP). The cultured Colon 26 cells were treated with 50% FBS as described above and then harvested for RNA extraction at 0, 6, 12, 18, and 24 hours after 50% FBS treatment. Nontreated Colon 26 cells harvested at the same time points were used as the control. At 6 or 18 hours after serum treatment, cells were exposed to Tf-NGPE L-OHP (L-OHP, 0.4 mg/mL) for 3 hours. The Pt content in the DNA was measured using an inductively coupled plasma mass spectrometer (ICP-MS). To explore the dosing time–dependent difference in the internalization of Pt into tumor cells *in vivo*, tumor-bearing mice were injected with a single dose of Tf-NGPE L-OHP at 9:00 a.m. or 9:00 p.m. Plasma and tumor DNA samples were collected only once from individual mice at 1, 3, and 6 hours after injection. The plasma concentration of Pt and its content in tumor DNA were measured as described above. Then, tumor volumes were measured throughout the duration of the experiment.

RT-PCR analysis

Total RNA was extracted using RNAiso (TaKaRa). The cDNAs of mouse *TfR1* (NM011638), *TfR2* (NM015799), *c-Myc* (NM010849), and β-*actin* (NM007393) were synthesized using PrimeScript Reverse Transcriptase (TaKaRa), and the synthesized cDNAs were amplified using GoTaq Green Master Mix (Promega). The PCR products were run on 2% agarose gels. After staining with ethidium bromide, the gel was photographed using Polaroid-type film. The density of each band was analyzed using NIH image software on a Macintosh computer. To evaluate the quantitative reliability of RT-PCR, kinetic analysis of the amplified products was performed to ensure that signals were derived only from the exponential phase of amplification, as previously described (7, 17). We evaluated the validity of our semiquantitative PCR methods using real-time PCR. cDNA was prepared by reverse transcription of total RNA. Real-time PCR analysis was performed on diluted cDNA samples with SYBR Premix Ex Taq Perfect Real-Time (TaKaRa) using a 7500 Real-time PCR system (Applied Biosystems). In addition, as confirmation of RNA extraction from each tumor cell sample, the expression level of *Vegf* mRNA was measured (Supplementary Data S1).

Western blotting analysis

Nuclear or cytoplasmic proteins in tumor masses were extracted using NE-PER Nuclear and Cytoplasmic Extraction Reagents (Pierce Biotechnology). The protein concentrations were determined using a BCA Protein Assay kit (Pierce Biotechnology). The lysate samples were separated on 6% or 10% SDS-polyacrylamide gels and transferred to polyvinylidene difluoride membranes. The membranes were reacted with antibodies against TfR1 (Zymed Laboratories), c-MYC, CLOCK, β-actin (Santa Cruz Biotechnology), or RNA pol II (Abcam). The immunocomplexes were further reacted with horseradish peroxidase–conjugated secondary antibodies and visualized using Super Signal Chemiluminescent Substrate (Pierce Biotechnology). The membranes were photographed using Polaroid-type film, and the density of each band was analyzed using NIH image software on a Macintosh computer.

Construction of reporter and expression vectors

The 5′ flanking region of mouse *TfR1* (from bp +16 to +436; +1 indicates the transcription start site) gene was amplified using Elongase Enzyme mix (Invitrogen) using DNA extracted from Colon 26 cells. PCR was performed using the forward primer 5′-AGTTGAGCTC(*SacI*)GGCTTGGTGCAGCTCAGTTAGTAG-3′ and reverse primer 5′-ATGAGATATC(*Eco*RV)TAAATGTCCGTTGACACTAGTAACC-3′. The PCR products were purified and ligated into a pGL4 Basic vector (*TfR1*-Luc). The sequence of the CACGTG E-box (bp +290 to +295) on *TfR1*-Luc was mutated using a QuikChange site-directed mutagenesis kit (Stratagene). Expression vectors for mouse CLOCK, BMAL1, and c-Myc were constructed using cDNAs obtained from RT-PCR derived from mouse liver RNA. All coding regions were ligated into the pcDNA3.1 (+) vector (Invitrogen), as previously described (7). Protein expression levels from each expression vector in Colon 26 were assessed by Western blotting analysis (Supplementary Data S2).

Luciferase reporter assay

Colon 26 cells were seeded at 3×10^5 cells per well in six-well culture plates (BD Biosciences). After an 18-hour culture, the cells were transfected with 100 ng per well of reporter vector and 2 μg per well (total) of expression vector using Lipofectamine LTX reagent (Invitrogen). A 0.5-ng-per-well sample of phRL-TK vector (Promega) was also cotransfected as an internal control reporter. The total amount of DNA per well was adjusted by adding pcDNA3.1 vector (Invitrogen). At 24 hours posttransfection, cells were harvested and the cell lysate was analyzed using a dual-luciferase reporter assay system (Promega). The ratio of firefly luciferase activity to *Renilla* luciferase activity in each sample served as a measure of normalized luciferase activity.

Small interfering RNA

siRNA of the mouse *c-Myc* gene was designed using BLOCK-iT RNAi Designer (Invitrogen). The siRNA oligonucleotide sequences were as follows: siRNA control sense, 5′-UAGUGUGAGCACUGUGAUUCCUUGG-3′ and antisense 5′-CCAAGGAUCACAGUGCUCACACUA-3′; *c-Myc* siRNA sense 5′-UAGUCGAGGUC-AUAGUUCCUGUUGG-3′ and antisense 5′-CCAACAGGAACUAUGACCUCGACUA-3′. The oligonucleotides were transfected into Colon 26 cells at a final concentration of 20 nmol/L using Lipofectamine 2000 (Invitrogen).

Chromatin immunoprecipitation assays

Tumor masses were excised and treated with 1% formaldehyde for 5 minutes at room temperature to cross-link the chromatin, and the reaction was stopped by adding glycine to a final concentration of 0.125 mol/L. Each cross-linked sample was sonicated on ice and then incubated with antibodies against c-MYC, CLOCK, rabbit-IgG, or goat-IgG (Santa Cruz Biotechnology). Chromatin/antibody complexes were extracted using a protein G agarose kit (Roche). DNA was isolated using the Wizard SV Genomic DNA Purification System (Promega) and subjected to PCR using the following primers for the c-MYC binding site (E-box) of the *TfR1* promoter region, forward 5′-GTGACTCCCTTGTCAG-3′ and reverse 5′-CCGTGACACTAGTAACC-3′. For PCR analysis, PCR products were amplified for 40 or 45 cycles. PCR products were run on an agarose (3%) gel, including 0.2 μg/mL ethidium bromide, and analyzed using the NIH image software.

Determination of L-OHP (Pt) concentration

Plasma samples were obtained by centrifugation at 3,000 rpm for 3 minutes and stored at −20°C until analysis. Tumor DNA was extracted using a Wizard Genomic DNA Purification kit (Promega). Measurements of the L-OHP (Pt) content in plasma and tumor DNA were made using ICP-MS at the Center of Advanced Instrumental Analysis, Kyushu University. ICP-MS is capable of detecting very small amounts of Pt. Plasma Pt concentration and its tumor DNA content were expressed as micrograms per milliliter and nanograms per nanogram of DNA, respectively.

Determination of the antitumor effect

Seven days after the inoculation of Colon 26 cells into mice, a single injection of Tf-NGPE L-OHP (L-OHP: 0, 7.5 mg/kg, i.v.) or vehicle (9% sucrose) was given to tumor-bearing mice at 9:00 a.m. or 9:00 p.m. This dosage of Tf-NGPE L-OHP was selected based on a preliminary study (Supplementary Data S3). In all mice, the tumor volumes were measured every 3 days throughout the duration of the experiment.

Statistical analysis

ANOVA was used for multiple comparisons, and Scheffe's test was used for comparison between two groups. A 5% level of probability was considered significant.

Results

Twenty-four-hour rhythm in the expression of TfR1 in Colon 26 tumor masses

Two subtypes of TfR have been identified: TfR1 and TfR2. In implanted Colon 26 cells, *TfR1* but not *TfR2* was detectable, although *TfR2* was expressed in mouse liver (Supplementary Data S1B). The protein and mRNA levels of TfR1 in implanted Colon 26 cells showed a significant 24-hour rhythm, with higher levels during the early dark phase ($P < 0.05$; Fig. 1A and B). The increase and decrease in mRNA levels of *TfR1* seemed to cause the rhythm of TfR1 protein in Colon 26 tumor masses.

Regulation of the 24-hour rhythm in the expression of *TfR1* gene by c-MYC

Among these, c-MYC is a potent activator of *TfR1* gene transcription in mice and humans, and the transactivation effect was elicited through binding to the CACGTG E-box located in the first intron region (18, 19). In addition, CLOCK/BMAL1 heterodimers also bind cooperatively to CACGTG E-box sequences and regulate the rhythmic expression of their target genes (2). Thus, to establish the relevance of the biological clock system on the expression of *TfR1*, CLOCKΔ19 (CLOCK protein lacking transcriptional activity) was overexpressed in Colon 26 cells. Clock mutant mice have

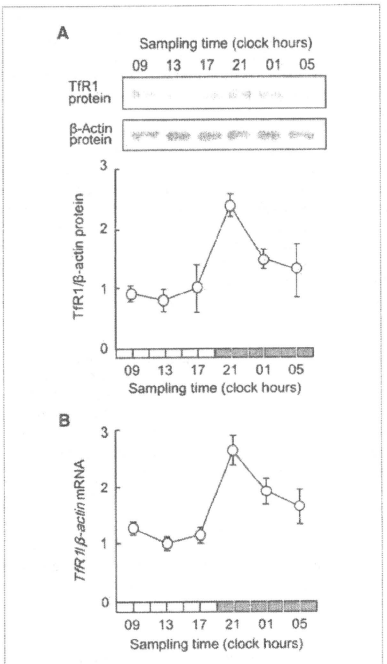

Figure 1. Twenty-four hour variation in the expression of TfR1 in Colon 26 tumor masses. A, temporal expression profile of TfR1 protein in tumor masses. The photographs show 24-h variation in TfR1 protein in implanted Colon 26 tumor cells. Cytoplasmic proteins were measured using each of the antibodies. Bottom, relative TfR1 protein levels. The data were normalized using β-actin as a control. Points, mean (n = 3, P < 0.01, ANOVA); bars, SEM. B, temporal expression profile of *TfR1* mRNA in tumor masses. The data are normalized using β-*actin* as a control. Points, mean (n = 6, P < 0.01, ANOVA); bars, SEM.

a point mutation in exon 19 of the *Clock* gene and exhibit low-amplitude rhythms in the expression of various genes (20). *TfR1* and *c-Myc* expression levels were low in CLOCKΔ19 overexpressing Colon 26 cells (Supplementary Data S4). Next, we tested whether these transcription factors participate in regulation of the rhythmic expression of *TfR1* gene in Colon 26 cells. Cotransfection of *TfR1*-Luc with c-MYC expression constructs resulted in an 8.1-fold increase in promoter activity, whereas CLOCK/BMAL1 had little effect on the transcriptional activity of the *TfR1* gene (Fig. 2B). The transactivation effect of c-MYC on *TfR1* reporters was dependent on the E-box element located from bp +290 to +295 because mutation of the CACGTG sequence to AAGCTT reduced transcriptional activation by c-MYC from 8.1- to 1.5-fold.

Several compounds and high concentration serum have been shown to induce and/or synchronize circadian gene expression in cultured cells (21). Thus, to elucidate the role of c-MYC in the circadian regulation of *TfR1* expression, the temporal expression profiles of *TfR1* mRNA in c-MYC–downregulated Colon 26 cells were investigated after 50% FBS treatment. Brief exposure of control scrambled siRNA-transfected cells to 50% FBS resulted in the oscillation of *TfR1* mRNA levels with a period length of ~24 hours (Fig. 3A). On the other hand, the protein levels of c-MYC were decreased and the mRNA levels of *TfR1* failed to show a significant 24-hour oscillation after the treatment of *c-Myc* siRNA–transfected cells with 50% FBS (Fig. 3B and C). These results suggested that c-MYC is required for generating the time-dependent variation in *TfR1* mRNA expression.

The transcription of *c-Myc* is regulated by components of the circadian clock, and its mRNA levels in mouse liver and bones have been shown to exhibit a significant 24-hour oscillation (22). The protein levels of c-MYC in Colon 26 cells implanted in mice also showed obvious 24-hour oscillations with higher levels around the early dark phase and lower levels during the early light phase, whereas there was no obvious 24-hour variation in the protein levels of CLOCK in the tumor

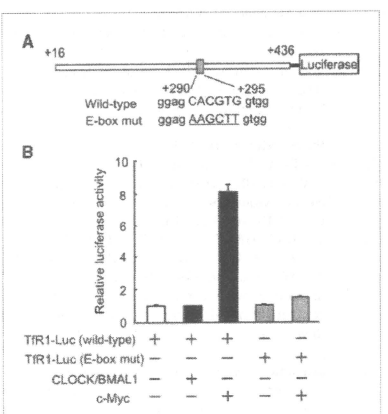

Figure 2. Influence of CLOCK/BMAL1 and c-MYC on transcription of the mouse *TfR1* gene. A, schematic representation of the mouse *TfR1* promoter. The numbers on both sites, the distance (bp) from the transcription start site (+1) included in the luciferase reporter construction. The numbers of nucleotide residues below the box, the positions of the E-box. The underlined nucleotide residues, the mutated sequence of the E-box. B, wild-type or E-box–mutated *TfR1* gene reporter plasmids (*TfR1*-Luc) were cotransfected with expression constructs encoding CLOCK/BMAL1 or c-MYC. Columns, mean (n = 3); bars, SEM.

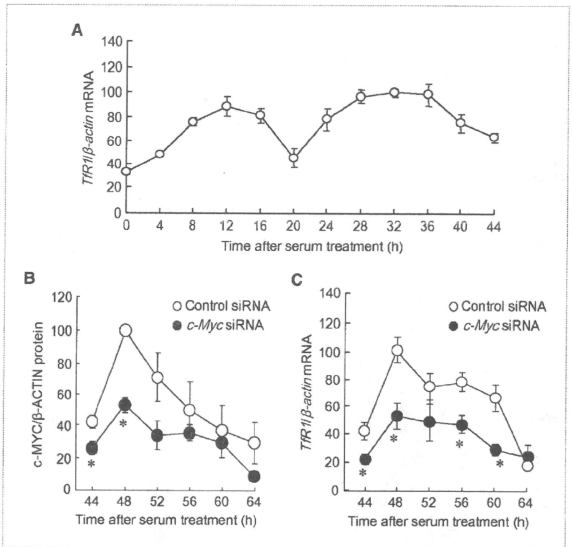

Figure 3. Influence of the downregulation of c-MYC on the rhythmic expression of *TfR1* mRNA in Colon 26 cells. A, temporal accumulation of *TfR1* mRNA in Colon 26 cells after 50% serum shock. The data are normalized using β-*actin* as a control. Points, mean ($n = 3$, $P < 0.01$, ANOVA); bars, SEM. Data are plotted relative to the 0-h value after 50% serum shock. B, temporal accumulation of c-MYC protein in control cells or c-Myc knockdown cells after 50% serum shock. Colon 26 cells were transfected with scrambled siRNA (control siRNA) or specific siRNA for c-Myc (c-Myc siRNA). Crude cell extracts were measured by Western blotting analysis. The data were normalized using β-actin as a control. Points, mean ($n = 3$, control cells; $P < 0.01$, ANOVA); bars, SEM. *; $P < 0.05$, when compared with the value for the control siRNA group at the corresponding times. C, temporal accumulation of *TfR1* mRNA in control cells or *c-Myc* knockdown cells. The mRNA levels of *TfR1* were determined at the indicated time points after serum treatment. Points, mean ($n = 3$, control cells; $P < 0.01$, ANOVA); bars, SEM. *, $P < 0.05$, when compared with the value for the control siRNA group at the corresponding times.

cells (Fig. 4A). The results of chromatin immunoprecipitation analysis revealed that endogenous c-MYC in Colon 26 cells bound to the E-box element in the intron region of *TfR1* gene (Fig. 4B). Of particular note, the binding amounts of c-MYC increasedat the time of day corresponding to the peak of *TfR1* mRNA expression (see Fig. 1B), suggesting that the time-dependent binding of c-MYC to the E-box in *TfR1* gene underlies its rhythmic expression. In addition, the mRNA levels of a prototypical c-MYC–regulated gene, telomerase reverse transcriptase (23), in Colon 26 cells implanted in mice also showed time-dependent variation (Supplementary Data S5).

Relationship between the rhythmic expression of TfR1 and time dependency of Pt incorporation into tumor DNA

Tf-NGPE L-OHP is a transferrin-conjugated liposome encapsulating L-OHP, a diaminocyclohexane Pt antitumor agent, which forms adducts with DNA. Tf-NGPE L-OHP binds to TfR, which is expressed on the plasma membrane and can internalize Pt into the cell.[3] Thus, to explore the function of internalization into the cell through transferrin in the rhythmic expression of TfR1, we investigated the temporal profile of *TfR1* gene expression and incorporation of Pt into tumor DNA in synchronized and desynchronized Colon 26 cells. A brief exposure of cultured Colon 26 cells to 50% FBS medium for 2 hours induced an oscillation in the expression of *TfR1* mRNA (Fig. 5A). The mRNA levels of *TfR1* peaked at 18 hours after treatment of the cells with 50% FBS. The oscillation of *TfR1* mRNA levels was also found on day 3 after serum treatment (see Fig. 3). The amount of Pt incorporated into the DNA of serum-shocked cells after treatment with Tf-NGPE L-OHP increased significantly at the time point corresponding to the peak in the level of TfR1 protein ($P < 0.05$; Fig. 5B). In contrast, in nontreated cells, neither the mRNA and protein levels of TfR1 nor Pt incorporation showed significant time-dependent variations (Fig. 5A and B), suggesting that the oscillation in the

[3] Our unpublished data.

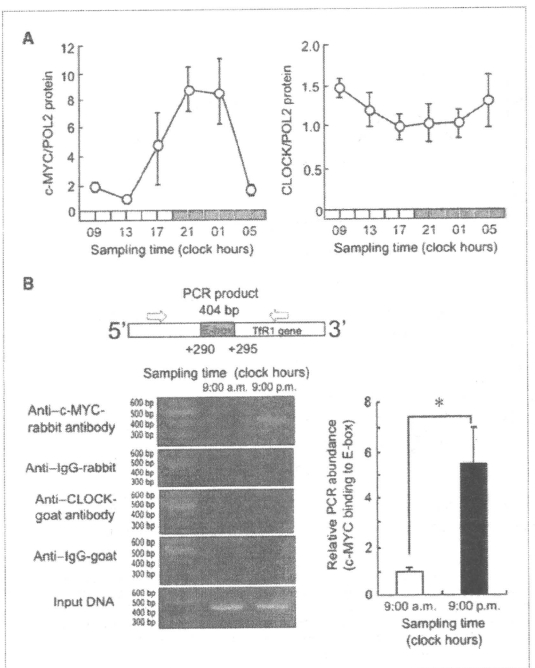

Figure 4. Time-dependent changes in the binding of endogenous c-MYC to the E-box element in the *TfR1* gene. A, temporal expression profiles of protein levels of c-MYC and CLOCK in implanted Colon 26 tumor masses. POL2 protein was used as an internal control whose expression was constant throughout the day. The data are normalized using POL2 as a control ($P < 0.01$, ANOVA). CLOCK protein did not show an obvious variation. Points, mean ($n = 3$); bars, SEM. B, left, temporal profiles of the binding of endogenous c-MYC to the *TfR1* gene in Colon 26 cells implanted in mice. Right, the quantification of temporal changes in the binding of c-MYC to the *TfR1* gene in Colon 26 cells implanted in mice. The mean value of each assay at 9:00 a.m. was set at 1. Columns, mean ($n = 3$); bars, SEM. *; $P < 0.05$ for the comparison between the two groups.

expression of TfR1 underlies the time-dependent change in Pt incorporation into tumor DNA.

Influence of dosing time on the ability of Tf-NGPE L-OHP to inhibit tumor growth

The plasma Pt concentration decreased gradually after a single injection of 7.5 mg/kg Tf-NGPE L-OHP (i.v.) at both dosing times, but the Pt concentration in plasma at 3 hours after Tf-NGPE L-OHP injection was significantly higher in mice injected with the drug at 9:00 a.m. than at 9:00 p.m. (Fig. 6A, left). On the other hand, Pt incorporation into DNA in tumor cells at 3 and 6 hours after Tf-NGPE L-OHP injection was significantly higher in mice injected with the drug at 9:00 p.m. than at 9:00 a.m. (Fig. 6A, right). We also attempted to determine the Pt contents in tumor DNA at over 6 hours after Tf-NGPE L-OHP injection, but accurate assessment was difficult, probably due to L-OHP–induced apoptotic or necrotic tumor cell death.

A significant antitumor effect of Tf-NGPE L-OHP was observed when tumor-bearing mice were injected i.v. with a single dose of 7.5 mg/kg L-OHP (Supplementary Data S3). Thus, the dosage was set at 7.5 mg/kg to investigate whether the antitumor effect of Tf-NGPE L-OHP was altered depending on its dosing time. The growth of tumor cells was significantly suppressed by the administration of Tf-NGPE L-OHP (7.5 mg/kg, i.v.). The antitumor effects were more potent in mice injected with the drug at 9:00 p.m. than in those that received it at 9:00 a.m. (Fig. 6B). Fifteen days after injection of the drug, the tumor volume in mice injected with Tf-NGPE L-OHP at 9:00 p.m. was significantly smaller than that in mice injected at 9:00 a.m. ($P < 0.05$).

Discussion

TfR1 is a key cell surface molecule that regulates the uptake of iron-bound transferrin (8). It has been shown that correlation exists between the number of surface TfR1 and the rate of cell proliferation. TfR1 expression is higher in tumor cells than in normal cells. Thus, intracellular targeting using iron-saturated Tf as a ligand for TfR-mediated endocytosis has attracted attention. In this study, the protein abundance of TfR1 on Colon 26 tumor cells implanted in mice showed a clear 24-hour oscillation. The rhythmic phase of TfR1 protein

paralleled that of its mRNA levels. However, the mechanisms of transcriptional rhythm of TfR1 were unclear.

The molecular circadian clock operates at a cellular level and coordinates a wide variety of physiologic processes (24). CLOCK/BMAL1 heterodimers activate the transcription of *Per*, *Cry*, and *Dec* genes through CACGTG E-box enhancer elements (8). The results of luciferase reporter assays and chromatin immunoprecipitation experiments revealed that the CACGTG E-box located in the first intron of the mouse *TfR1* gene was unable to respond to CLOCK/BMAL1 heterodimers. In contrast, as reported previously (19), c-MYC could bind to the E-box of the mouse *TfR1* gene and activate its transcription. The amount of endogenous c-MYC protein binding to the mouse *TfR1* gene E-box fluctuated in a time-dependent manner. The binding of c-MYC to the E-box increased at the time corresponding to the peak of *TfR1* mRNA expression, suggesting that c-MYC acts as a regulator of circadian expression of the *TfR1* gene in Colon 26 tumor cells. This hypothesis was also supported by the present findings that the amplitude of the *TfR1* mRNA rhythm in serum-shocked Colon 26 cells was decreased by the down-regulation of c-MYC. On the other hand, CLOCK protein did not bind to the *TfR1* gene E-box. This may account for the unresponsiveness of the *TfR1* gene to CLOCK/BMAL1 heterodimers. The sequence surrounding the E-box and its location had a marked influence on the transcriptional activity of CLOCK/BMAL1 (6). In fact, a CT-rich *cis*-acting element of the mouse vasopressin gene confers robust CLOCK/BMAL1 responsiveness on an adjacent E-box (25). The absence of such a CT-rich *cis*-acting element around the E-box may result in the inability of CLOCK/BMAL1 to transactivate the mouse *TfR1* gene.

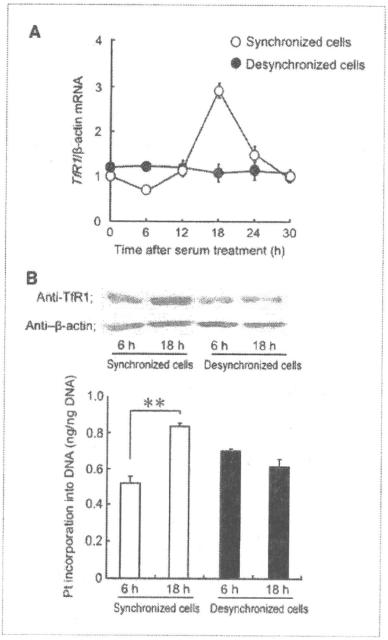

Figure 5. Influence of rhythmic changes in the expression of TfR1 on intratumoral delivery of L-OHP by Tf-NGPE liposomes. A, the temporal expression profile of *TfR1* mRNA in synchronized (○) or unsynchronized (●) Colon 26 cells. Cultured Colon 26 cells were synchronized by exposure to 50% FBS for 2 h. Points, mean (n = 3, synchronized cells; $P < 0.05$, ANOVA); bars, SEM. B, the photographs show temporal expression of TfR1 protein in synchronized or unsynchronized Colon 26 cells. Bottom, that temporal profile of Pt incorporation into DNA in synchronized or unsynchronized Colon 26 cells. Cells were exposed to Tf-NGPE L-OHP (L-OHP: 0.4 mg/mL) for 3 h at 6 or 18 h after the serum treatment, and then the amounts of Pt incorporated into tumor DNA were measured. Columns, mean (n = 3); bars, SEM. *, $P < 0.05$ for the comparison between the two time points.

Because the rhythmic phase of c-MYC protein abundance in Colon 26 cells correlated with the time dependency of its binding to the *TfR1* gene E-box, the oscillation in c-MYC protein levels may cause the 24-hour rhythm in the expression of downstream genes by rhythmic binding to their DNA response elements. In fact, *mTERT* mRNA in implanted Colon 26 tumor also showed time-dependent variation. In addition, *c-Myc* is regulated by clock genes, as indicated by previous results (26). *TfR1* and *c-Myc* expression levels were low in CLOCKΔ19-overexpressing Colon 26 cells. Although the E-box of the *TfR1* gene did not respond to CLOCK/BMAL1, the molecular components of the circadian clock may indirectly regulate the expression of the *TfR1* gene in Colon 26 cells.

It was reported previously that L-OHP could accumulate in tumor masses following delivery using Tf-PEG liposomes (16). TfR-targeting liposomes also bind to TfR on tumor cell surfaces and are internalized into the cells by receptor-mediated endocytosis. In this study, to evaluate the function of the 24-hour oscillation in TfR1, Tf-NGPE liposomes were used as a targeting carrier for intratumoral delivery of L-OHP. This TfR-targeting liposomal DDS exhibited similar pharmacokinetic properties to Tf-PEG liposomes, and i.v. administration of L-OHP encapsulated within Tf-NGPE liposomes lead to the accumulation of a high concentration of L-OHP in tumors as much as Tf-PEG liposomes.[4] The amount of Pt in tumor DNA after Tf-NGPE L-OHP injection increased at the times of day when TfR1 was abundant on the tumor surface in this study. This notion was also supported by *in vitro* findings that the time dependency of Tf-NGPE liposome–delivered L-OHP into tumor cells disappeared in the absence of the oscillation in TfR1 expression. These findings suggest that the oscillation in the expression of TfR1 underlies the dosing time–dependent changes in the internalization into

[4] Our unpublished data.

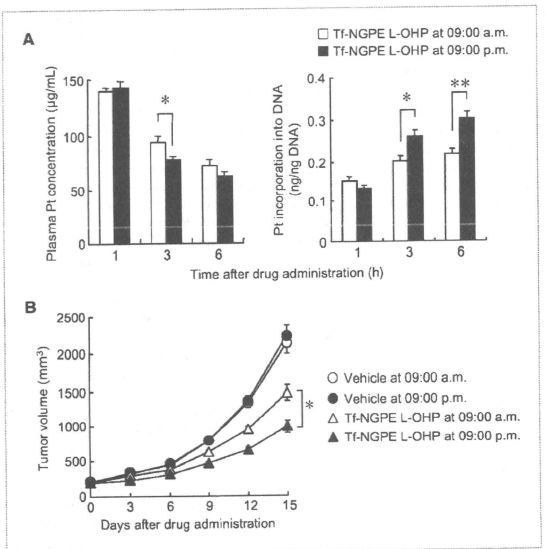

Figure 6. Influence of dosing time on the ability of Tf-PEG L-OHP to inhibit tumor growth in mice. Colon 26 tumor–bearing mice were injected i.v. with a single dose of Tf-NGPE L-OHP (L-OHP: 7.5 mg/kg) or vehicle (9% sucrose) at 9:00 a.m. or 9:00 p.m. A, dosing time–dependent differences in the intratumoral delivery of L-OHP by Tf-NGPE liposomes were examined. Plasma Pt concentration (left) and Pt incorporation into tumor DNA (right) were measured at the indicated times after an injection of Tf-NGPE L-OHP. Columns, mean (n = 5); bars, SEM; **, $P < 0.01$; *, $P < 0.05$ for comparison between the two groups. B, dosing time–dependent difference in the antitumor effect of Tf-NGPE L-OHP. Points, mean (n = 8–10); bars, SEM; *, $P < 0.05$ for comparison between the two dosing times.

the cells by receptor-mediated endocytosis. In addition, after a single injection of Tf-NGPE L-OHP, the antitumor effect of the drug varied according to its dosing time. The dosing time dependency of the antitumor effect seemed to be caused by time-dependent changes in the intratumoral delivery of L-OHP by TfR-targeting liposomes.

In the present study, it was shown that the 24-hour rhythm of TfR1 expression in colon cancer cells was controlled by c-MYC, and the cyclical accumulation of TfR1 caused dosing time–dependent changes in the intratumoral delivery of L-OHP by receptor-mediated endocytosis. Identification of the circadian properties of molecules that are targeted by ligand-directed DDS may aid the choice of the most appropriate time of day for their administration.

Disclosure of Potential Conflicts of Interest

The authors disclose no conflicts.

Grant Support

Grants-in-Aid for Scientific Research on Priority Areas "Cancer" (S.O. 20014016) from the Ministry of Education, Culture, Sport, Science and Technology of Japan, for Scientific Research (B; S.O. 21390047), for Challenging Exploratory Research (S.O. 21659041), and for the Encouragement of Young Scientists (N.M. 20790137) from the Japan Society for the Promotion of Science.

The costs of publication of this article were defrayed in part by the payment of page charges. This article must therefore be hereby marked *advertisement* in accordance with 18 U.S.C. Section 1734 solely to indicate this fact.

Received 01/18/2010; revised 06/07/2010; accepted 06/07/2010; published OnlineFirst 07/13/2010.

References

1. Stephan FK, Zucker I. Circadian rhythms in drinking behavior and locomotor activity of rats are eliminated by hypothalamic lesions. Proc Natl Acad Sci U S A 1972;69:1583–6.
2. Alvarez JD, Sehgal A. Circadian rhythms: finer clock control. Nature 2002;419:798–9.
3. Gekakis N, Staknis D, Nguyen HB, et al. Role of the CLOCK protein in the mammalian circadian mechanism. Science 1998;280:1564–9.
4. Kume K, Zylka MJ, Sriram S, et al. mCRY1 and mCRY2 are essential components of the negative limb of the circadian clock feedback loop. Cell 1999;98:193–205.
5. Preitner N, Damiola F, Lopez-Molina L, et al. The orphan nuclear receptor REV-ERBα controls circadian transcription within the positive limb of the mammalian circadian oscillator. Cell 2002;110:251–60.
6. Sato TK, Yamada RG, Ukai H, et al. Feedback repression is required for mammalian circadian clock function. Nat Genet 2006;38:312–9.

7. Koyanagi S, Kuramoto Y, Nakagawa H, et al. A molecular mechanism regulating circadian expression of vascular endothelial growth factor in tumor cells. Cancer Res 2003;63:7277–83.
8. Daniels TR, Delgado T, Helguera G, Penichet ML. The transferrin receptor part II: targeted delivery of therapeutic agents into cancer cells. Clin Immunol 2006;121:159–76.
9. Sorokin LM, Morgan EH, Yeoh GC. Transformation-induced changes in transferrin and iron metabolism in myogenic cells. Cancer Res 1989;49:1941–7.
10. Niitsu Y, Kohgo Y, Nishisato T, et al. Transferrin receptors in human cancerous tissues. Tohoku J Exp Med 1987;153:239–43.
11. Calzolari A, Oliviero I, Deaglio S, et al. Transferrin receptor 2 is frequently expressed in human cancer cell lines. Blood Cells Mol Dis 2007;39:82–91.
12. Kawabata H, Nakamaki T, Ikonomi P, Smith RD, Germain RS, Koeffler HP. Expression of transferrin receptor 2 in normal and neoplastic hematopoietic cells. Blood 2001;98:2714–9.
13. Röhrs S, Kutzner N, Vlad A, Grunwald T, Ziegler S, Müller O. Chronological expression of Wnt target genes Ccnd1, Myc, Cdkn1a, TfRc, Plf1 and Ramp3. Cell Biol Int 2009;33:501–8.
14. Papahadjopoulos D, Allen TM, Gabizon A, et al. Sterically stabilized liposomes: improvements in pharmacokinetics and antitumor therapeutic efficacy. Proc Natl Acad Sci U S A 1991;88:11460–4.
15. Ishida O, Maruyama K, Tanahashi H, et al. Liposomes bearing polyethyleneglycol-coupled transferrin with intracellular targeting property to the solid tumors *in vivo*. Pharm Res 2001;18: 1042–8.
16. Suzuki R, Takizawa T, Kuwata Y, et al. Effective anti-tumor activity of oxaliplatin encapsulated in transferrin-PEG-liposome. Int J Pharm 2008;346:143–50.
17. Ohdo S, Koyanagi S, Suyama H, Higuchi S, Aramaki H. Changing the dosing schedule minimizes the disruptive effects of interferon on clock function. Nat Med 2001;3:356–60.
18. Holloway K, Sade H, Romero IA, Male D. Action of transcription factors in the control of transferrin receptor expression in human brain endothelium. J Mol Biol 2007;365:1271–84.
19. O'Donnell KA, Yu D, Zeller KI, et al. Activation of transferrin receptor 1 by c-Myc enhances cellular proliferation and tumorigenesis. Mol. Cell Biol 2006;26:2373–86.
20. Oishi K, Miyazaki K, Kadota K, et al. Genome-wide expression analysis of mouse liver reveals CLOCK-regulated circadian output genes. J Biol Chem 2003;278:41519–27.
21. Takiguchi T, Tomita M, Matsunaga N, Nakagawa H, Koyanagi S, Ohdo S. Molecular basis for rhythmic expression of CYP3A4 in serum-shocked HepG2 cells. Pharmacogenet Genomics 2007;17: 1047–56.
22. Wittekindt NE, Hörtnagel K, Geltinger C, Polack A. Activation of *c-myc* promoter P1 by immunoglobulin κ gene enhancers in Burkitt lymphoma: functional characterization of the intron enhancer motifs κB, E box 1 and E box 2, and of the 3′ enhancer motif PU. Nucleic Acids Res 2000;28:800–8.
23. Reymann S, Borlak J. Transcription profiling of lung adenocarcinomas of *c-myc*-transgenic mice: identification of the *c-myc* regulatory gene network. BMC Syst Biol 2008;2:46.
24. Weaver ReppertSM. Coordination of circadian timing in mammals. Nature 2002;418:935–41.
25. Muñoz E, Brewer M, Baler R. Modulation of BMAL/CLOCK/E-Box complex activity by a CT-rich *cis*-acting element. Mol Cell Endocrinol 2006;252:74–81.
26. Fu L, Pelicano H, Liu J, Huang P, Lee C. The circadian gene Period2 plays an important role in tumor suppression and DNA damage response *in vivo*. Cell 2002;111:41–50.

JRR-4 facility for animal irradiation experiments

K. Endo[1], T. Yamamoto[1,2], K. Nakai[1], Hiroaki Kumada[2], Y. Shibata[1], A. Matsumura[1]

[1]*Department of Neurosurgery, Graduate School of Comprehensive Human Science, University of Tsukuba 1, Tennoudai 1-1-1, Tsukuba City, Japan*

[2]*Department of Radiation Oncology, Graduate School of Comprehensive Human Science, University of Tsukuba 2, Tennoudai 1-1-1, Tsukuba City, Japan*

Abstract

A small animal irradiation facility is critical for providing optimal radiation dose distributions for pre-clinical studies. Animal neutron irradiation experiments cause many problems to solve, as the achievements of the permissions from the animal care office and using committee. At the same time, it is necessary to make radioprotection controls and to take care of radiation waste management. Animal irradiation was possible only few days per month because of shared nuclear reactor. As JRR-4 has no beam shutter, exclusive use of reactor was needed. To avoid this time consuming procedure, we constructed a simple facility for animal irradiation at JRR-4.

This system consists of some animal holders, a manual loader and some visual monitors. Animal holders can be filled with anesthetic gas, so that the mice are under general anesthesia during the irradiation. Rearing facilities were constructed into the radiation controlled area. Tumor control test by boron agents and neutron irradiation were put into practice. Unfortunately, a problem at the reactor caused a neutron outage which will last for about 3 years. This paper focuses on simulated neutron distribution and simulated absorbed dose in the animal body.

Keywords: BNCT, JAEA, JRR-4, animal irradiation

1. Introduction

The small animal irradiation facility at the Institute for Reactor Research should be able to ethically treat animals, and should have the proper equipment, personnel and problem-solving capabilities, necessary for such kind of studies. The management of such a facility requires much more than the routine control of the radioactive materials and the radioprotection of the users and animals.

Despite the complexities and expense of running such a facility, experiments evaluating the effects of radiation alone or in combination with other agents on tumor proliferation in small animals are indispensable for drug development and for the improvement of irradiation techniques.

The following accomplishments using the JAEA (Japan Atomic Energy Agency) research reactor JRR-4 (JAEA Research Reactor-4) were so far achieved:

The reactor was available only few days during the year, we examined current situations, obstacles and issues involved in the development of the small animal irradiation experiments in the JRR-4 furnace, and reported on the neutron beam distribution and the simulation of the dose absorbed by the animal body.

2. Materials and Methods

The irradiation system consists of animal holders, a manual loader and visual monitors. Animal holders can be filled with the anesthetic gas, so that mice can be irradiated under anesthesia, allowing for a safer and a more accurate dose administration. Breeding facilities were constructed into the radiation-controlled area. Tumor size control and neutron irradiation tests using boron agents were established and safely carried out.

Using the newly designed animal irradiation devices, 4-6 animals can be irradiated at a time using the rails method, which is the newly designed animal irradiation devices as figure a. In addition, it also allows for a more uniform irradiation of the animals (Figure a).

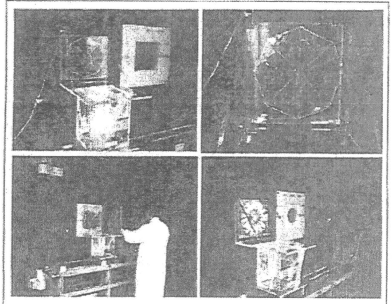

a: The newly designed animal irradiation devices.

Using our system with the JCDS (JAEA Computational Dosimetry System) that Kumada (2003) developed for dose calculation, the location for animal irradiation was reproduced and the dose was simulated. To determine the partial irradiation, we tested the irradiation setup most suitable to treat that tumor models. And we also examined the influence of an acrylic cover, boron rubber, and the LiF cover belt.

3. Results

We found that the 30 mm cover was sufficient (Figure b). However the 46 mm cover is naturally a better screen. The 15 mm thick cover is too thin, and the flux in the body of the mouse was double if compared with the cover 46 mm thick. The 30 mm cover is still flexible enough to be used as a shield for the mouse. Moreover, the importance of the shield thickness was confirmed for other cover materials, including the acrylic fiber and LiF.

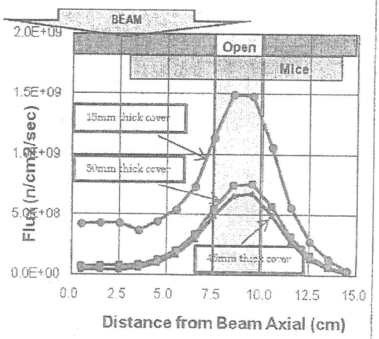

b: Differences of beam flux by the thickness of cover material.

Even if the beam is stopped directly by the shield, because of the characteristic of the neutron flux, it can be deflected and reach other non-covered area, parts of the body, such as the head and the legs. So we must develop the new device to avoid this problem in the future.Because of the flux in the peripheral zone of the 20 cm beam was largely depressed, the flux in the peripheral zone was the same as that from the 15 cm beam. Therefore, no major difference was observed between the 20 cm and 15 cm beams in this evaluation (Figure c).

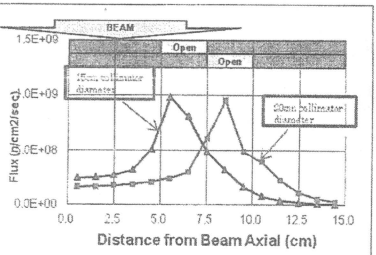

c: Differences of beam flux distribution by 15 cm and 20 cm collimator diameter with cover material.

A variety of collimator diameters and cover materials were examined to determine which would ensure the most uniform neutron beam irradiation of the animals. The best collimator diameter sets were determined to be 20 cm and 15 cm, and LiF cover material was 46 mm thick to protect the animals. After examining the different parameters, including irradiation conditions, duration of anesthesia, and driving time, the most suitable irradiation time was found to be 17 minutes, using the epithermal neutron beam.

4. Exclusive driving

Exclusive driving is indispensable to small animal irradiation, but it is difficult to perform under time limitations. In addition, it is necessary to start and stop the nuclear reactor, and this could cause potential problems with the staff security. Several issues remain to be solved regarding radioactivity management and the animal protection.

We should cooperate with the laboratory of university extension, a domestic study group about animal irradiation and the research reactor using section in JAEA which can be used domestically in Japan for animal irradiation studies. We had to overcome numerous problems in order to establish an effective animal irradiation device with the exclusive use of the research reactor.

5. Conclusion

Unfortunately, the neutron outage has not been available for about the past 3 years. This paper focused on simulated neutron flux distribution and evaluated how various neutron doses can be delivered to different parts of the body in mice. When the JRR-4 facility, will be available again, we plan to verify the feasibility of the system and its applications for animal experiments.

References

Kumada H., Yamamoto K., Torii Y., Matsumura A., Yamamoto T., Nose T., Nakagawa Y., Kageji T., Uchiyama J., 2003. Development of the JAERI Computational Dosimetry System (JCDS) for Boron Neutron Capture Therapy (Cooperative Research). JAERI-Tech 2003-002, 1-49.

Development of a functional liposome modified a novel lipid analog for BNCT

Makoto Shirakawa[1], Tetsuya Yamamto[1], Kei Nakai[1], Humiyo Yoshida[1], Takao Tsurubuchi[1], Masahide Matsuda[1], Yohei Yamamoto[1], Yuusaku Yokoyama[2], Akira Matsumura[1]

[1] *University of Tsukuba, Graduate School of Comprehensive Human Sciences, Functional and Regulatory Medical Sciences , 1-1-1 Tennodai, Tsukuba, Ibaraki 305-8575, Japan*

[2] *Faculty of Pharmaceutical Sciences, Toho University, 2-2-1 Miyama Funabashi, Chiba 274-8510, Japan*

Abstract

We aimed at securing sufficient concentrations of ^{10}B in BNCT by developing a new drug delivery system. We have designed and developed a novel lipid analog and succeeded in using it to develop the new boron component liposome. It consisted of three different kinds of amino acid derivatives and two fatty acids, and could react directly with the peptide synthesized first on resin by Fmoc solid-phase synthesis. In this study, lipid analog conjugated with HIV-TAT peptide (domain of human immunodeficiency virus TAT protein) and boronophenylalanine (BPA) was synthesized and successfully incorporated into liposomes. This liposome showed *in vitro* the boron concentration of 156 times in comparison with BSH (sodium borocaptate) solution. This shows superior cell introduction ability of the liposome. Furthermore, as for this liposome including BSH solution experimented on by a similar method, improvement of the further boron concentration was developed.

Keywords: boron neutron capture therapy (BNCT), boron delivery system (BDS), liposome, HIV-TAT

1. Introduction

Boron neutron capture therapy (BNCT) is a tumor-selective radiation modality which depends on a sufficient cellular uptake of Boron (^{10}B) followed by irradiation with a beam of thermal or epithermal neutrons. ^{4}He and ^{7}Li particles are produced during the neutron capture reaction and damage DNA, which leads to cell killing. Regarding BNCT, the short radiation range of ^{4}He and ^{7}Li particles is decisive for the distribution of ^{10}B. Thus, successful treatment of cancer by BNCT requires the selective delivery of relatively large amounts of ^{10}B compound to malignant cells. The estimated boron concentration required for effective therapy is in the range of 20–30 μg ^{10}B per g tissue. However there have been no ideal boron compounds that fulfill the conditions of low toxicity, water solubility, and low distribution in normal tissue. Therefore, we aimed at securing sufficient concentrations of ^{10}B in BNCT by developing a new drug delivery system.

2. Materials and methods

2.1. Synthesis of lipopeptide

Lipopeptide conjugated with HIV-TAT peptide and boronophenylalanine (BPA) was synthesized on TGS-RAM resin by the Fmoc solid-phase synthesis method using an automatic peptide synthesizer (Shimadzu PSSM-8 Peptide Synthesizer Simultaneous Multiple) (**Figure 1**). Tryptophan residue was added at the N-terminus of HIV-TAT peptide as a fluorescence probe. BPA was coupled arbitrarily. Then, Fmoc-AEEA (9-fluorenylmethoxycarbonyl-8-amino-3,6-dioxaoctanoic acid, linker domain), 11 Fmoc-Asp-OtBu (hydrophilic domain), and

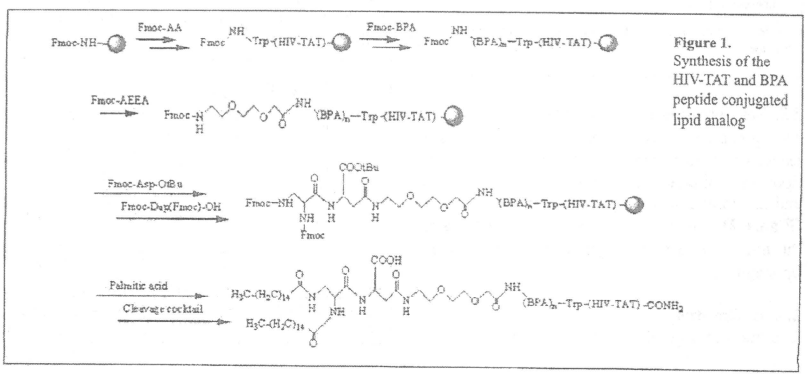

Figure 1. Synthesis of the HIV-TAT and BPA peptide conjugated lipid analog